Transient Analysis and Control Strategies for a Quad-Inverter Multiphase Multilevel Motor Drive in Faulty Conditions

Gabriele Grandi[1], Padmanaban Sanjeevkumar[2] and Yasser Gritli[1]

1. Department of Electrical Engineering, University of Bologna, Bologna 40136, Italy

2. Department of Electrical & Electronics, National Institute of Technology-Puducherry, Karaikal 609 605, India

Abstract: In this paper, post-fault-tolerant control strategies for quad-inverter multiphase-multilevel induction motor drives are investigated. More specifically, four standard two-level three-phase VSIs (voltage source inverters) supplying the open-end windings of a dual three-phase induction motor is considered, quadrupling the power capability of a single VSI with given voltage and current ratings. In healthy conditions, the control algorithm is able to generate multi-level voltage waveforms, equivalent to the ones of a three-level inverter and to share the total motor power among the four dc sources in each switching period. This sharing capability is investigated under post-fault operating conditions, when one VSI must be completely insulated due to a severe failure on it. In this case, the conversion power unit can operate with a reduced power rating by a proper modulation of the remaining three VSIs. The whole ac motor drive has been numerically implemented, and the effectiveness of the proposed control strategies under healthy and post-fault operating conditions have been proved.

Key words: Dual three-phase motor, multi-level inverter, multi-phase motor drive, multi-phase fault, post-fault-tolerance, space vector modulation.

1. Introduction

Fault-tolerability in ac traction systems is a key item with high-voltage/high-current applications, where availability and reliability of performances are mandatory. In specific, for this type of application, induction motors operate continuously in dynamic conditions, requiring frequent start/stop with rapid speed variations. Subsequently, the drives are regularly subjected to abuse of over-current surges and voltage over-swings. Recent research carried out on different failure possibilities in induction motor drives by industrials and experts have revealed that 21% are related to the stator windings and its configuration. Several phenomenons can affect its reliability, such as mechanical and/or thermal stress, leading to severe failure possibilities such as inter-turn short-circuits, line-to-line, line-to-ground, multi-phase line-to-ground and multi-phase faults. A detailed analysis of these types of fault and its propagation and diagnosis can be found in Refs. [1-3].

Among various innovation and approaches in literatures relating to fault-tolerant performances, multi-phase ac machine technologies have been widely recognized as a viable solution [4]. More specifically, multi-phase drives are very advantageous in high power ac traction applications, thanks to its inherent active redundant structure, which improve considerably the system reliability. It takes only two phases (having independent currents) to create a fundamental magnetomotive force distribution rotating at the supply frequency, so a machine with m-phases

---

Corresponding author: Gabriele Grandi, professor, research fields: power electronics, photovoltaic energy conversion. E-mail: gabriele.grandi@unibo.it.

can continue to operate at reduced power in a controlled manner, with m-2 open phases. Therefore, multi-phase inverters together with multi-phase ac machines have been proved as a fruitful solution, also providing high power ratings with current-limited devices [4, 5]. Other investigations to increase the power ratings have focused their efforts on multi-level inverters, being advantageous in terms of high voltages that can be provided using sources and switching devices with reduced voltage ratings. Additional benefits such as reduced harmonic distortion and lower *dv/dt* in the output voltages make this solution very suitable for industry applications [6, 7]. Other topologies based on passive or/and active semiconductors have been proposed for the same purposes, but the lower reliability still remains their major drawback [8, 9]. A large reliability investigation of inverter topologies has revealed that its estimated MTBFs (mean time between failures) is of about two years [10].

Among the proposed modern topologies, the conventional two-level three-phase voltage source inverter still remains a mature technology. However, all types of inverters are still vulnerable to different potential anomalies, leading to an imminent total failure. Recent survey on inverters has revealed that 31%-37.9% of failures are caused by power parts [10] and the main failure mechanisms in modern power modules with IGBT devices for high-power applications can be found in Ref. [11]. Most potential sources of failures based on power devices, capacitors and gate control are detailed in Ref. [12]. In this sense, innovative topologies based on a proper arrangement of conventional two-level three-phase VSIs (voltage source inverters) to realize both multi-phase [13, 14] and multi-level [15-18] inverters have been investigated. The reduced cost of both inverter and motor due to conventional slot/winding configurations, and modularity of the whole conversion structure, with high reliability in power layout, are the main advantages of such topologies.

Motivated by the above performances, and considering the low reliability of the commercial inverters becoming more and more integrated, which reduce considerably its maintainability or reconfiguration [12], a novel structure based on a dual three-phase open-ends winding motor (asymmetric six-phase induction machine) has been considered in this paper. The power supply consists of four standard two-level three-phase VSIs having insulated dc sources to prevent circulation of zero-sequence current components and improving the reliability. The topology of the investigated structure, with its corresponding equivalent circuit in terms of three-phase space vectors, is reported by Figs. 1a and 1b, respectively. It is important to note that the structure is easy scalable to 9, 12 or higher number of phases multiple of three. A modulation strategy has been utilized to regulate each couple of two-level VSIs such as the three-level inverter given by Ref. [18], providing proper multi-level voltage waveforms for each three-phase stator winding. Furthermore, the proposed control algorithm allows total motor power to be shared among the four dc sources with three degrees of freedom [19-21].

In perspective view, the proposed contribution is devoted to investigate inherent active redundancy of the used quad-inverter, under one, two or three failed inverters, to ensure system operability in degraded mode given by Ref. [22]. In this paper, the post-fault operating condition under one failed inverter is investigated. The resulting two degrees of freedom allow either balanced power sharing between the two three-phase motor windings, with minimization of power losses, or balanced power sharing among the three remaining dc sources. Some preliminary experimental results by a six-phase passive load are given in Ref. [23].

2. Basics of the Quad-Inverter Induction Motor Drive

Multiple space vectors are considered to represent the variables of the whole six-phase system consisting
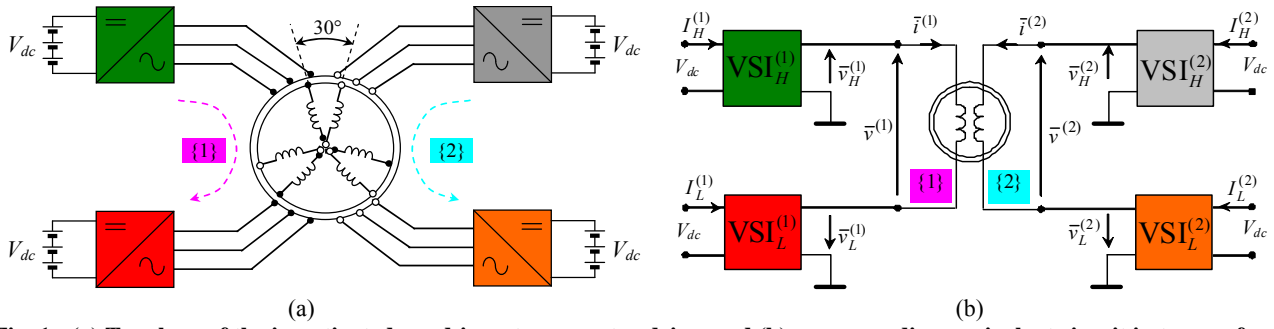
(a)   (b)

Fig. 1 (a) Topology of the investigated quad-inverter ac motor drive; and (b) corresponding equivalent circuit in terms of three-phase space vectors (healthy inverters).

of the dual three-phase machine supplied by four three-phase VSIs with insulated dc supplies. In particular, the asymmetric six-phase space vector transformations introduced in Refs. [13, 14] are considered.

Considering the investigated topology (Fig. 1a) and its corresponding equivalent circuit (Fig. 1b), the behavior of the dual three-phase induction machine having sinusoidal distributed stator windings can be described in terms of multiple space vectors by the following equations, written in a stationary reference frame [14]:

$$\bar{v}_{S1} = R_S\,\bar{i}_{S1} + \frac{d\bar{\varphi}_{S1}}{dt} \quad \bar{\varphi}_{S1} = L_{S1}\,\bar{i}_{S1} + M_1\,\bar{i}_{R1} \quad (1)$$

$$0 = R_R\,\bar{i}_{R1} - j\,p\,\omega_m\bar{\varphi}_{R1} + \frac{d\bar{\varphi}_{R1}}{dt} \quad \bar{\varphi}_{R1} = M_1\,\bar{i}_{S1} + L_{R1}\,\bar{i}_{R1} \quad (2)$$

$$\bar{v}_{S5} = R_S\,\bar{i}_{S5} + \frac{d\bar{\varphi}_{S5}}{dt} \quad \bar{\varphi}_{S5} = L_{S\ell}\,\bar{i}_{S5} \quad (3)$$

$$T = 3\,p\,M_1\,\bar{i}_{S1}\cdot j\,\bar{i}_{R1} \quad (4)$$

where, p is the pole pairs number, ω_m is the rotor angular speed, and the subscripts S and R denote stator and rotor quantities, respectively. It should be noted that the sinusoidal spatial distribution of the magnetic field in the air gap is mainly generated by the space vectors $\bar{i}_{S1}$ and $\bar{i}_{R1}$, whereas $\bar{i}_{S5}$ does not contribute to the air gap field.

The total motor power P can be expressed by Ref. [21]:

$$P = P^{(1)} + P^{(2)} = \frac{3}{2}\Big[\big(\bar{v}_H^{(1)} + \bar{v}_L^{(1)}\big)\cdot\bar{i}^{(1)} + \big(\bar{v}_H^{(2)} + \bar{v}_L^{(2)}\big)\cdot\bar{i}^{(2)}\Big] \quad (5)$$

being $P^{(1)}$ and $P^{(2)}$ the individual powers of the two three-phase stator windings {1} and {2} given by:

$$\begin{cases} P^{(1)} = \frac{3}{2}\bar{v}^{(1)}\cdot\bar{i}^{(1)} \\ P^{(2)} = \frac{3}{2}\bar{v}^{(2)}\cdot\bar{i}^{(2)} \end{cases} \quad (6)$$

and the stator winding voltages $\bar{v}^{(1)}$ and $\bar{v}^{(2)}$ can be written as the sum of voltages of the individual inverters "H" and "L" as:

$$\begin{cases} \bar{v}^{(1)} = \bar{v}_H^{(1)} + \bar{v}_L^{(1)} \\ \bar{v}^{(2)} = \bar{v}_H^{(2)} + \bar{v}_L^{(2)} \end{cases} \quad (7)$$

In the proposed system, the power sharing among the four dc sources is characterized by three degrees of freedom, expressed by the three coefficients k_i, $k_v^{(1)}$, and $k_v^{(2)}$ [21].

The first coefficient k_i concerns with current and power sharing between the two three-phase windings {1} and {2}:

$$\begin{cases} \bar{i}^{(1)} = 2k_i\,\bar{i}_{S1} \\ \bar{i}^{(2)} = 2\alpha^{-1}(1 - k_i)\,\bar{i}_{S1} \end{cases} \quad (8)$$

$$\begin{cases} P^{(1)} = P_H^{(1)} + P_L^{(1)} \cong k_i\,P \\ P^{(2)} = P_H^{(2)} + P_L^{(2)} \cong (1 - k_i)\,P \end{cases} \quad (9)$$

The second $k_v^{(1)}$ and third $k_v^{(2)}$ coefficients are related to the voltage and power sharing between the two inverters "H" and "L" which supply each three-phase winding:

$$\begin{cases} \bar{v}_H^{(1)} = k_v^{(1)}\,\bar{v}^{(1)} \\ \bar{v}_L^{(1)} = \big(1 - k_v^{(1)}\big)\,\bar{v}^{(1)} \end{cases} \quad \begin{cases} \bar{v}_H^{(2)} = k_v^{(2)}\,\bar{v}^{(2)} \\ \bar{v}_L^{(2)} = \big(1 - k_v^{(2)}\big)\,\bar{v}^{(2)} \end{cases} \quad (10)$$

$$\begin{cases} P_H^{(1)} = k_v^{(1)}\,P^{(1)} \\ P_L^{(1)} = \big(1 - k_v^{(1)}\big)P^{(1)} \end{cases} \quad \begin{cases} P_H^{(2)} = k_v^{(2)}\,P^{(2)} \\ P_L^{(2)} = \big(1 - k_v^{(2)}\big)P^{(2)} \end{cases} \quad (11)$$

Note that, to equally share the motor power among the four inverters, i.e., 25% of the total power for each dc source, all sharing coefficients k_i, $k_v^{(1)}$ and $k_v^{(2)}$ must be set to 1/2.

In order to synthesize the voltage vectors $\bar{v}^{(1)}$ and $\bar{v}^{(2)}$, a proper multi-level SVM algorithm must be applied to satisfy also the power sharing between the two windings [18]. With reference to Fig. 2a, due to the symmetry of the outer hexagon, the analysis can be restricted to one of its six sectors (i.e., OAB), similarly to the case of conventional three-phase SVM algorithm. Furthermore, the main triangle OAB is divided in four identical equilateral triangles. The reference voltage $\bar{v}^{(1)}$ lays in one of these triangles, leading to four relevant cases. By the basic SVM principle, the components $\bar{v}_H^{(1)}$ and $\bar{v}_L^{(1)}$ can be generated by selecting adjacent vectors. The switch configurations corresponding to these vectors can not be applied in an arbitrary sequence if proper multi-level voltage waveforms are desired, i.e., the reference voltage $\bar{v}^{(1)}$ should be generated by using the NTV (nearest three vectors) approach [21]. For this purpose, the method introduced in Ref. [18] has been implemented.

The same considerations are valuable for the voltage reference $\bar{v}^{(2)}$.

3. The Proposed Post-Fault-Tolerant Strategies

Integrated cooling technologies are widely employed in commercial inverter applications for high power ac traction system, having advantages such as ease-of-use, miniaturization and compactness in traction systems. However, the non-maintainability due to the compact packaging and the reduced thermal dissipation justifies the reduced reliability of the inverters [8, 11, 12].

Independently to the technology adopted, the inverters are still mainly subjected to several failures due to:
- dc-link electrolytic capacitor;
- dc bus voltage sensor;
- power semiconductor (short circuit or open circuit);
- control and driver circuits.

Commonly known by its rapid propagation, is leading to severe degrees of damage for the whole system.

For these reasons, whenever one among the four inverters is affected by the above failures, most of the times the concerned inverter can be considered as totally damaged and must be removed. The failed inverter should be disconnected from both the motor and the dc source (battery), e.g., using bypass switches. Then, the developed control system is adapted in a manner that the ac motor drive machine still continues to operate in post-fault conditions.

Under the considered post-fault configuration, the proposed control strategy allows continuity of operation, but with reduced degree of freedom in the power sharing among the dc sources: from three degrees, under healthy conditions, to two.

In fact, supposing the fault occurs on inverter $\mathrm{VSI}_L^{(1)}$, as represented in Fig. 3, the corresponding dc source must be insulated, and the three output phases must be short circuited to allow current circulation on stator

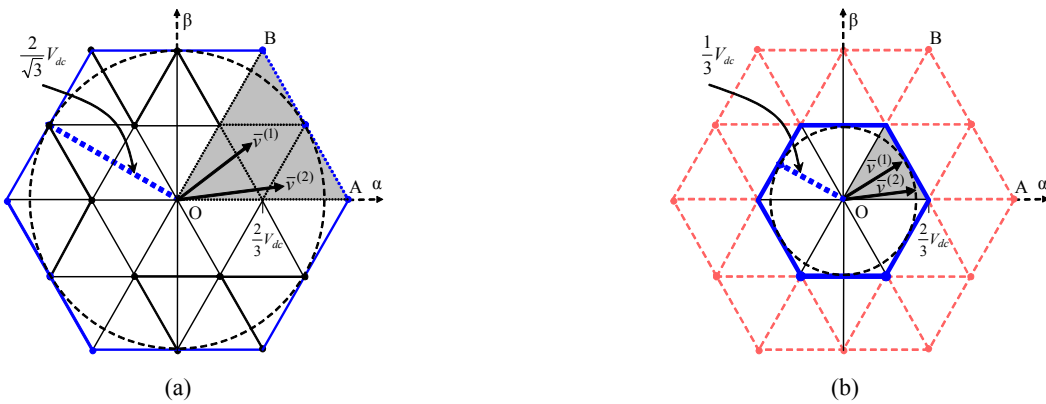(a)   (b)

Fig. 2   Voltage space vectors generated by inverters H and L for the stator windings {1} and {2} under (a) healthy, conditions and (b) one failed inverter.
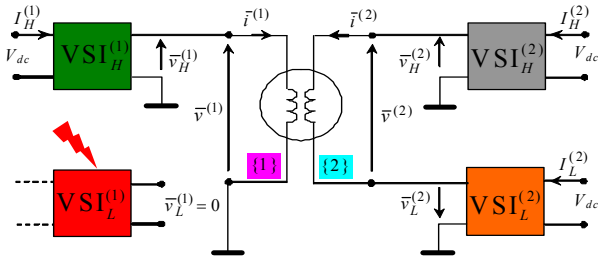
Fig. 3 Equivalent circuit of the post-fault configuration, in terms of three-phase space vectors, with one failed inverter, $v_L^{(1)} = 0$.

winding {1}. The open-end winding configuration of the motor now collapse to traditional three-phase star connection for stator winding {1}, and the entire voltage for stator winding {1}, $\bar{v}^{(1)}$, must be provided by inverter $VSI_H^{(1)}$. Whereas the voltage for stator winding {2}, $\bar{v}^{(2)}$, is provided by inverters $VSI_H^{(2)}$ and $VSI_L^{(2)}$.

Then, according to Eq. (10), the post-fault operating conditions can be summarized as:

$$\begin{cases} \bar{v}_L^{(1)} = 0 \\ \bar{v}_H^{(1)} = \bar{v}^{(1)} \end{cases} \quad \Longleftrightarrow \quad k_v^{(1)} = 1 \quad (12)$$

Taking into account Eqs. (9), (11) and (12), the individual inverter powers are now be expressed as:

$$\begin{cases} P_L^{(1)} = 0 \\ P_H^{(1)} = k_i P \end{cases} \quad \begin{cases} P_L^{(2)} \cong (1-k_i)(1-k_v^{(2)}) P \\ P_H^{(2)} \cong (1-k_i) k_v^{(2)} P \end{cases} \quad (13)$$

Being $k_v^{(1)}$ imposed by the fault, the remaining two degree of freedoms are now represented by $k_v^{(2)}$ (i.e., power (voltage) sharing between healthy inverters $VSI_H^{(2)}$ and $VSI_L^{(2)}$) and k_i (i.e., power (current) sharing between the two three-phase winding {1} and {2}). In this paper, condition (12) will be used in numerical simulations to represent the post-fault conditions instead of using additional bypass switches for creating star connection on the faulty inverter and complete insulation and for current circulation.

The first relevant consequence of the fault in one inverter is that the maximum output voltage for one of the two three-phase stator windings is halved. As a consequence, since the two stator windings share the same magnetic circuit and have the same induced

electromagnetic force, the maximum voltage of the other stator winding halved as well, leading to a 50% reduction of the whole maximum motor power, from $2/\sqrt{3}V_{dc}$ to $1/\sqrt{3}V_{dc}$, as emphasized in Fig. 2b.

This condition is summarized in Fig. 4, with reference to the torque versus speed characteristics in healthy (green line) and faulty (red line) operating conditions.

As an example, the operating point ① can be implemented only in healthy conditions, whereas the operating points ② and ③ can be implemented also in post-fault conditions (the last one with a flux weakening to reduce the required stator winding voltage).

Different strategies can be introduced to realize the post-fault operating conditions, with three healthy VSIs. In this paper will be considered the two relevant cases of minimization of power losses and symmetrical power sharing among the three healthy VSIs (i.e., among the corresponding three dc sources).

3.1 Balanced Power Sharing between the Two Three-Phase Stator Motor Windings and Minimization of Power Losses

As known, a balanced current sharing between the two three-phase windings leads to minimum stator copper losses. This can be simply implemented in post-fault conditions by setting $k_i = 1/2$, with arbitrary voltage sharing coefficient $k_v^{(2)}$ to synthesize $v^{(2)}$. Although the usage of both $VSI_H^{(2)}$ and $VSI_L^{(2)}$ allows an active redundancy, it is not optimal from the point of view of the inverter losses, involving two inverters when the desired output voltage could be synthesized with just one of them.

For this reason, the provision of a passive redundancy with one inverter for the winding {2} still considerably improve the reliability of the post-fault configuration but it reduces the whole converter losses. In this case, inverter $VSI_H^{(1)}$ can operates just with inverter $VSI_H^{(2)}$, whereas the output voltage of inverter $VSI_L^{(2)}$ is set to zero, or vice versa, leading to exactly
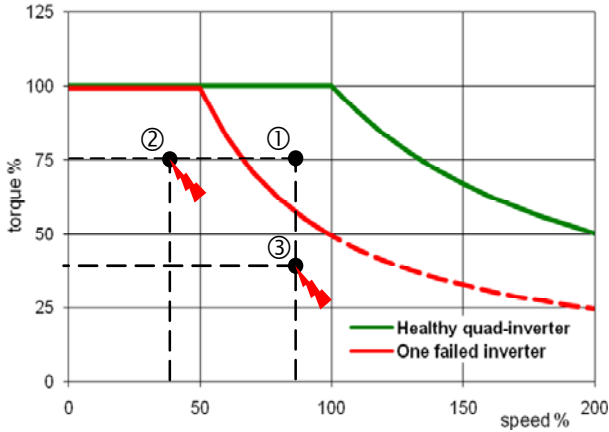
Fig. 4 Operating points under test in the torque versus speed diagram for healthy (4 VSIs) and one failed inverter (3 VSIs) conditions.

the same operating performances of the motor. The open-end windings configuration of the motor now collapse to traditional three-phase star connections for both stator windings. Voltage and power Eqs. (9)-(11), in addition to the fault condition (12), can now be summarized as:

$$\begin{cases} \bar{v}_L^{(2)} = 0 \\ \bar{v}_H^{(2)} = \bar{v}^{(2)} \end{cases} \qquad \Longleftrightarrow \qquad k_v^{(2)} = 1 \qquad (14)$$

$$\begin{cases} P_L^{(1)} = 0 \\ P_H^{(1)} = \frac{1}{2}P \end{cases} \qquad \Longleftrightarrow \qquad \begin{cases} P_L^{(2)} = 0 \\ P_H^{(2)} = \frac{1}{2}P \end{cases} \qquad k_i = \frac{1}{2} \ (15)$$

3.2 Balanced Power Sharing among the Three Healthy VSIs

Further step in this post-fault investigation, point of interest is to share the total motor power symmetrically among the three healthy inverters, i.e., among the three remaining dc sources. This behavior is recommended for battery supplied traction systems, in which the balanced charge status of batteries can be considered as a crucial issue. In order to implement a balanced power sharing among the three dc power supplies, an unbalanced power sharing between the two three-phase windings {1} and {2} must be introduced. In particular, one third of the total motor power must be supplied by each VSI, leading to the following voltage and power equations, according to Eqs. (9)-(13):

$$\begin{cases} \bar{v}_L^{(2)} = \frac{1}{2}\bar{v}^{(2)} \\ \bar{v}_H^{(2)} = \frac{1}{2}\bar{v}^{(2)} \end{cases} \qquad \Longleftrightarrow \qquad k_v^{(2)} = \frac{1}{2} \qquad (16)$$

$$\begin{cases} P_L^{(1)} = 0 \\ P_H^{(1)} = \frac{1}{3}P \end{cases} \qquad \Longleftrightarrow \qquad \begin{cases} P_L^{(2)} = \frac{1}{3}P \\ P_H^{(2)} = \frac{1}{3}P \end{cases} \qquad k_i = \frac{1}{3} \quad (17)$$

In the next section, simulation results under healthy and post-fault operating conditions, using balanced and unbalanced power sharing approaches, are presented and discussed.

4. Results of the Developed Control Strategies

For the purpose of investigation studies and to verify the effectiveness of the proposed post-fault control strategies, the whole system has been designed, implemented and numerically tested by means of the PLECS simulation package in the MATLAB environment under healthy and one failed inverter conditions. For the induction motor, the model is implemented with the parameters given in Table 1. The value of the four dc bus voltages (V_{dc}) is set to 155 V and switching frequency of each VSI is set to 5 kHz.

4.1 Investigation Performances during Healthy Condition (Operating Point ①)

In this simulation test, the system is analyzed in healthy state conditions in the whole interval (90 ms) considering the operating point ① in Fig. 4 (speed 1,200 rpm, torque 38 Nm). Balanced behavior is introduced by setting all the share coefficients to 1/2 as depicted in Fig. 5, i.e., the electrical power is equally shared among the four healthy VSIs. The electromagnetic torque T is depicted in Fig. 6.

Fig. 7 shows, from top-to-bottom, the waveforms of artificial line-to-neutral voltages of the first-phase, $v_{H1}^{(1)}$, $v_{L1}^{(1)}$, $v_{H1}^{(2)}$ and $v_{L1}^{(2)}$ (green, red, grey and orange traces, respectively). The time averaged voltage values are also depicted on the corresponding diagrams. It can be clearly noticed that the time averaged voltages are almost sinusoidal (fundamental components) with the same amplitude and with a proper phase shift (i.e., 180° between the two voltages on the same winding,

Table 1   Motor parameters.

P_{rated}	=	8	kW	R_S	=	0.51	Ohm
$I_{S, rated}$	=	16	A_{rms}	R_R	=	0.42	Ohm
$V_{S,rated}$	=	125	V_{rms}	L_{S1}	=	58.2	mH
$\omega_{S,rated}$	=	$2\pi \times 50$	rad/s	L_{R1}	=	58.2	mH
P	=	2	(pairs)	M_1	=	56	mH
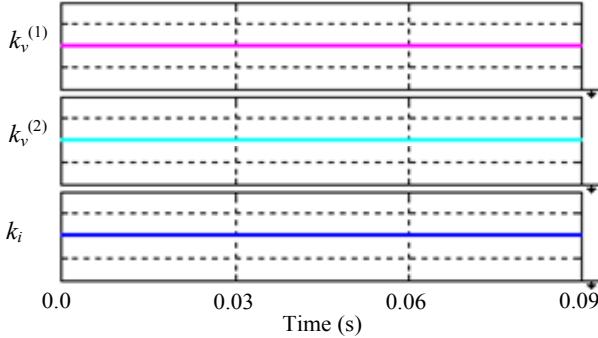
Fig. 5   Voltage and current sharing coefficients (0.25 units/div).
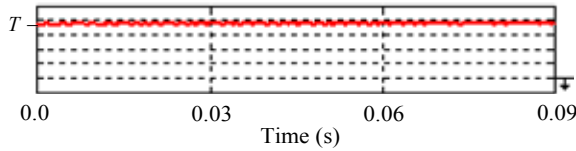
Fig. 6   Torque behavior in steady-state and healthy condition (10 Nm/div).
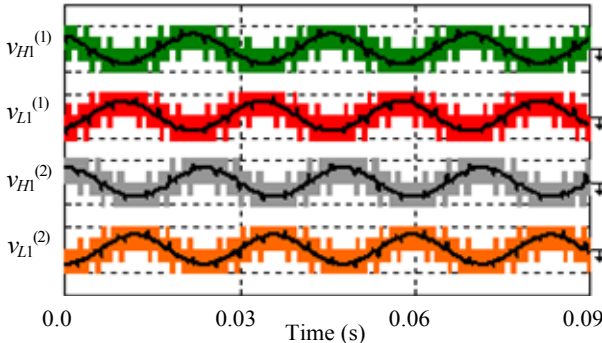
Fig. 7   Artificial line-to-neutral voltages (first-phase) with their time averaged components (100 V/div). From top-to-bottom: dual-inverter {1}: H green and L red traces, dual-inverter {2}: H gray and L orange traces.

and 30° between the voltages on different windings).

The stator windings voltages of the first-phase along with their time averaged values are depicted in Fig. 8, from top-to-bottom, $v_1^{(1)}$ and $v_1^{(2)}$ (purple and turquoise traces, respectively). As expected, proper multi-level stepped waveforms appear with nine levels, being the modulation index greater than 50% (outer hexagon shown in Fig. 2a), and a phase shift of 30° is noticed.
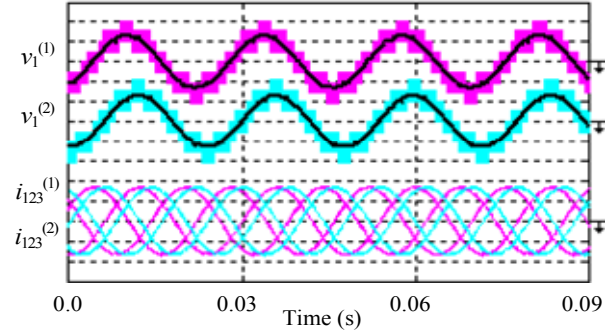
Fig. 8   Stator variables on first-phase in windings {1} and {2}. From top-to-bottom: voltages with time averaged components (purple and turquoise traces) (100 V/div), currents (purple and turquoise traces) (10 A/div).

The six stator winding currents are shown at the bottom side of Fig. 8, $i_1^{(1)}$, $i_2^{(1)}$, $i_3^{(1)}$ and $i_1^{(2)}$, $i_2^{(2)}$, $i_3^{(2)}$ ($i_{123}^{(1)}$, purple traces, and $i_{123}^{(2)}$, turquoise traces, respectively). Currents are almost sinusoidal, with the same amplitude, and correct 30° phase displacements.

Fig. 9 shows the dc currents of the four VSIs (currents from the dc supplies) $I_H^{(1)}$, $I_L^{(1)}$, $I_H^{(2)}$ and $I_L^{(2)}$ (green, red, grey and orange traces, respectively). Values are low-pass filtered ($t = 20$ ms) to emphasize the dc components. DC currents have the same value, proving the effectiveness of the modulation strategy in balanced operating conditions.

4.2 Investigation Performances during Post-Fault Conditions with One Failed Inverter

In the following two simulation tests, depicted in Figs. 10-19, the system is analyzed with healthy state in the first time interval (0-30 ms) considering the operating point ② in Fig. 4 (halved speed, 600 rpm, same torque, 38 Nm).

At the time instant $t = 30$ ms the fault on inverter $VSI_L^{(1)}$ occurs, and it is completely disabled by setting to 1 corresponding voltage sharing coefficient $k_v^{(1)}$, as expressed by Eq. (12). No further actions are taken in the second time interval (30-60 ms).

At the time instant $t = 60$ ms the two proposed post-fault strategies are applied, according to the description given in sub-Sections 3.1 and 3.2. No further actions are taken in this third time interval (60-90 ms). For the sake of readability of numerical
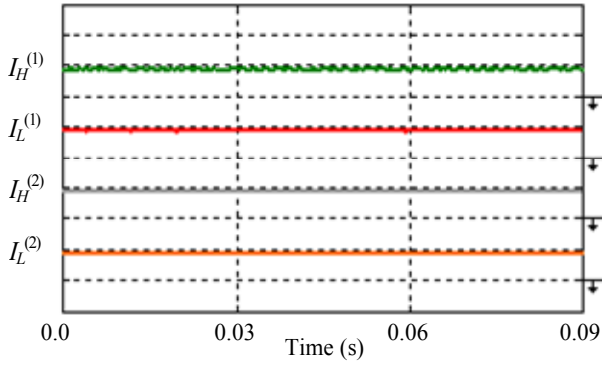
Fig. 9 DC currents of the four VSIs (low-pass filtered, t = 20 ms). From top-to-bottom: dual-inverter {1}: H green and L red traces; dual-inverter {2}: H grey and L orange traces (10 A/div).
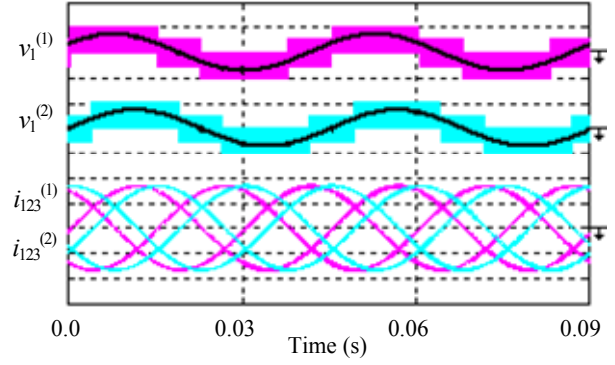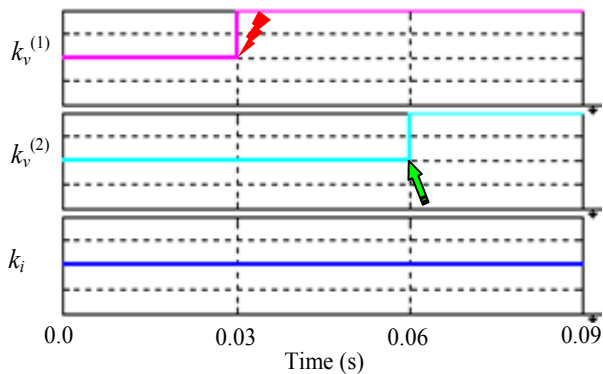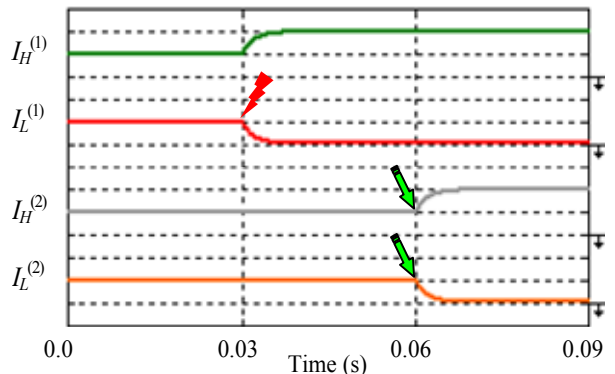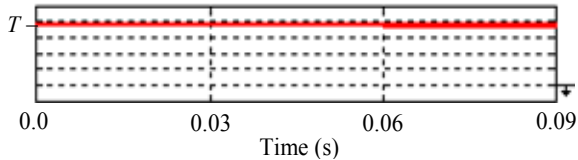

Fig. 10 Voltage and current sharing coefficients (0.25 units/div).

Fig. 11 Torque behavior in transient from healthy to post-fault conditions (10 Nm/div).
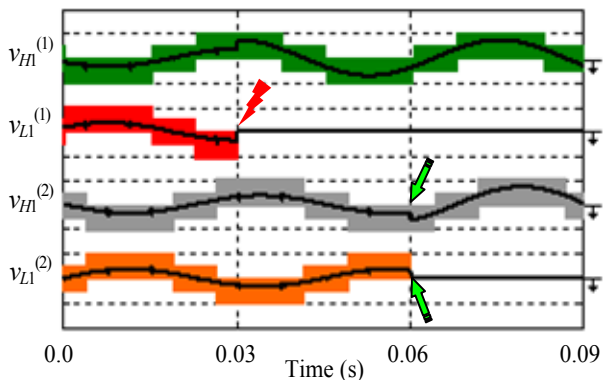

Fig. 12 Artificial line-to-neutral voltages (first-phase) with their time averaged components (100 V/div). From top-to-bottom: dual-inverter {1}: H green and L red traces; dual-inverter {2}: H gray and L orange traces.

Fig. 13 Stator variables on first-phase in windings {1} and {2}. From top-to-bottom: voltages with time averaged components (purple and turquoise traces) (100 V/div), currents (purple and turquoise traces) (10 A/div).

Fig. 14 DC currents of the four VSIs (low-pass filtered, τ = 20 ms). From top-to-bottom: dual-inverter {1}: H green and L red traces; dual-inverter {2}: H grey and L orange traces (5 A/div).

Fig. 15 Voltage and current sharing coefficients (0.25 units/div).

Fig. 16 Torque behavior in transient from healthy to post-fault conditions (10 Nm/div).

Fig. 17 Artificial line-to-neutral voltages (first-phase) with their time averaged components (100 V/div). From top-to-bottom: dual-inverter {1}: H green and L red traces; dual-inverter {2}: H gray and L orange traces.
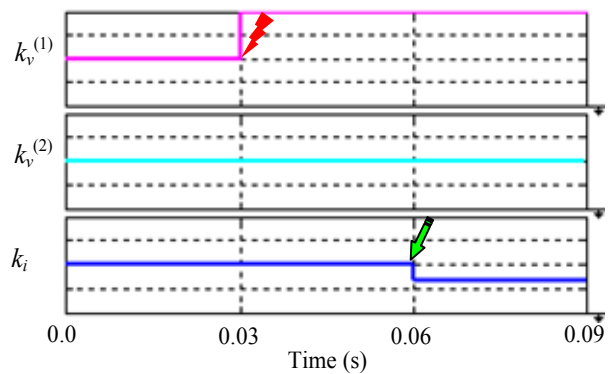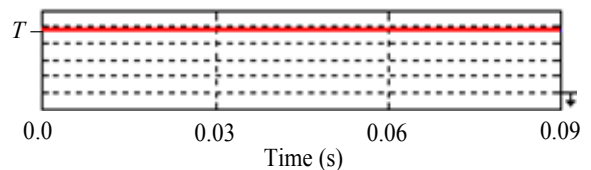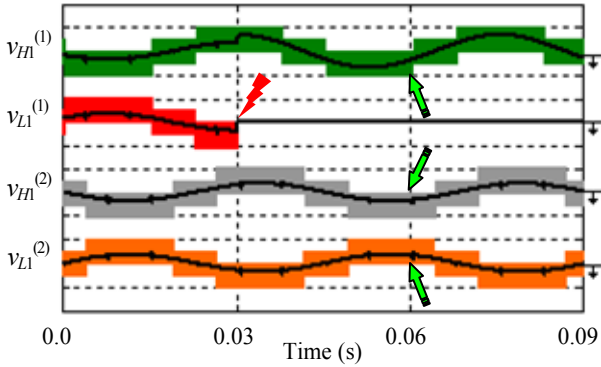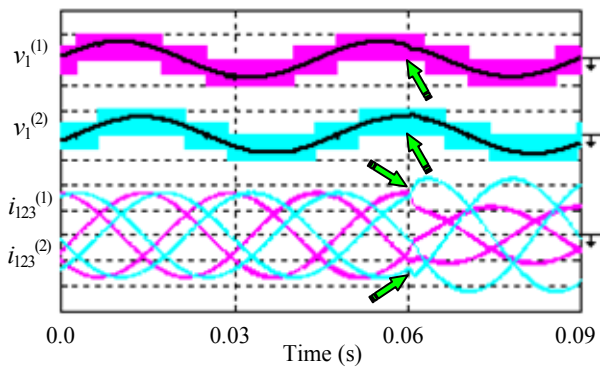

Fig. 18 Stator variables on first-phase in windings {1} and {2}. From top-to-bottom: voltages with time averaged components (purple and turquoise traces) (100 V/div), currents (purple and turquoise traces) (10 A/div).
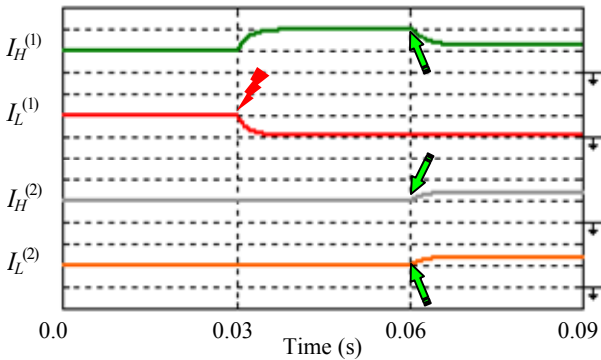

Fig. 19 DC currents of the four VSIs (low-pass filtered, τ = 20 ms). From top-to-bottom: dual-inverter {1}: H green and L red traces; dual-inverter {2}: H grey and L orange traces (5 A/div).

results, the fault instant is emphasized by a red shock arrow in Figs. 10-19, whereas the starting instant of the proposed control strategy is represented by a green straight arrow.

4.2.1 Balanced power sharing between the two three-phase stator motor windings (operating point②)

This first test during post-fault conditions was conducted to prove the effectiveness of the proposed control strategy when a balanced power sharing between the two windings is required, and minimization of inverter losses is realized by switching off one of the remaining three healthy VSIs.

Fig. 10 shows the variation of voltage and current sharing coefficients when the fault occurs (t = 30 ms, $k_v^{(1)}$ turns to 1) and when the first post-fault strategy is applied (t = 60 ms, $k_v^{(2)}$ turns to 1), according to conditions (14) and (15) introduced in sub-Section 3.1. The current sharing coefficient k_i remains unchanged.

Fig. 11 shows that the electromagnetic torque T is practically unaffected by transients in sharing coefficients, as it should be.

Fig. 12 shows, from top-to-bottom, the waveforms of artificial line-to-neutral voltages of the first-phase, $v_{H1}^{(1)}$, $v_{L1}^{(1)}$, $v_{H1}^{(2)}$ and $v_{L1}^{(2)}$ (green, red, grey and orange traces, respectively). The time averaged voltage values are also depicted on the corresponding diagrams. When the fault occurs on inverter $VSI_L^{(1)}$, the corresponding voltage $v_{L1}^{(1)}$ goes to zero, whereas the voltage on the other side of winding {1}, $v_{H1}^{(1)}$, doubles its value to provide for the missing winding voltage. Voltages $v_{H1}^{(2)}$ and $v_{L1}^{(2)}$ are unaffected by the fault, being applied to the other winding. As the first post-fault strategy is applied, $VSI_L^{(2)}$ is turned off by setting $v_{L1}^{(2)}$ to zero, and the voltage $v_{H1}^{(2)}$ doubles its value to provide for the missing voltage on winding {2}. The remaining active inverters $VSI_H^{(1)}$ and $VSI_H^{(2)}$ provide now the voltages $v_{H1}^{(1)}$ and $v_{H1}^{(2)}$ with same amplitudes and the proper 30° phase shift.

Fig. 13 shows the stator windings voltages of the first-phase along with their time averaged values, from top-to-bottom, $v_1^{(1)}$ and $v_1^{(2)}$ (purple and turquoise traces, respectively). As expected, multi-level stepped waveforms appear now with five levels, as for traditional two-level inverters, being the modulation index lower than 50% (inner hexagon shown in

Fig. 2b). The six stator winding currents are shown at the bottom side of Fig. 13, $i_{123}^{(1)}$ and $i_{123}^{(2)}$ (purple and turquoise traces, respectively). Note that both voltages and currents are practically unaffected by the fault and by the power sharing transients, as expected.

Fig. 14 shows the dc currents of the four VSIs (currents from the dc supplies) $I_H^{(1)}$, $I_L^{(1)}$, $I_H^{(2)}$ and $I_L^{(2)}$ (green, red, grey and orange traces, respectively). Values are low-pass filtered ($\tau = 20$ ms) to emphasize the dc components. Being the dc supply voltage V_{dc} constant during all transients, the dc currents well represent the individual powers supplied by the four VSIs. Then, it can be clearly seen as the total motor power is equally shared between $VSI_H^{(1)}$ and $VSI_H^{(2)}$ in this first post-fault control strategy, according to Eq. (15).

4.2.2 Balanced power sharing among the three healthy VSIs (operating point②)

This second test during post-fault conditions was conducted to prove the effectiveness of the proposed control strategy when a balanced power sharing among the remaining three healthy VSIs is required (i.e., balanced power sharing among the corresponding three dc sources).

Fig. 15 shows the variation of voltage and current sharing coefficients when the fault occurs ($t = 30$ ms, $k_v^{(1)}$ turns to 1) and when the second post-fault strategy is applied ($t = 60$ ms, k_i turns to 1/3), according to conditions (16) and (17) introduced in sub-Section 3.2. The voltage sharing coefficient $k_v^{(2)}$ remains unchanged. Fig. 16 shows that the electromagnetic torque T is practically unaffected by transients in sharing coefficients, as it should be.

Fig. 17 shows, from top-to-bottom, the waveforms of artificial line-to-neutral voltages of the first-phase, $v_{H1}^{(1)}$, $v_{L1}^{(1)}$, $v_{H1}^{(2)}$ and $v_{L1}^{(2)}$ (green, red, grey and orange traces, respectively). The time averaged voltage values are also depicted on the corresponding diagrams. When the fault occurs on inverter $VSI_L^{(1)}$, the corresponding voltage $v_{L1}^{(1)}$ goes to zero, whereas the voltage on the other side of winding {1}, $v_{H1}^{(1)}$, doubles

its value to provide for the missing winding voltage. Voltages $v_{H1}^{(2)}$ and $v_{L1}^{(2)}$ are unaffected by the fault, being applied to the other winding, as in the previous test. As the second post-fault strategy is applied, voltages $v_{H1}^{(1)}$, $v_{H1}^{(2)}$ and $v_{L1}^{(2)}$ just slightly change as a consequence of the change of the current sharing coefficient. In fact, just a small variation of stator winding voltages can be responsible of considerable currents changes.

Fig. 18 shows the stator windings voltages of the first-phase along with their time averaged values, from top-to-bottom, $v_1^{(1)}$ and $v_1^{(2)}$ (purple and turquoise traces, respectively). Also in this case, multi-level stepped waveforms appear with five levels, as for traditional two-level inverters, being the modulation index lower than 50% (inner hexagon shown in Fig. 2b). The slight voltage variation introduced by the current sharing coefficient change can now be better observed. The six stator winding currents are shown at the bottom side of Fig. 18, $i_{123}^{(1)}$ and $i_{123}^{(2)}$ (purple and turquoise traces, respectively). The current sharing coefficient change from 1/2 to 1/3 leads to an increase of currents on winding {2}, and to a decrease of currents on winding {1}, becoming ones the double of the others, according to Eq. (8).

Fig. 19 shows the dc currents of the four VSIs (currents from the dc supplies) $I_H^{(1)}$, $I_L^{(1)}$, $I_H^{(2)}$ and $I_L^{(2)}$ (green, red, grey and orange traces, respectively). Values are low-pass filtered ($\tau = 20$ ms) to emphasize the dc components. Since the dc current represents the individual power of each VSIs, it can be clearly seen as the total motor power is equally shared among inverters $VSI_H^{(1)}$, $VSI_H^{(2)}$ and $VSI_L^{(2)}$ in this second post-fault control strategy, according to Eq. (17).

5. Conclusions

An ac motor drive based on quad-inverter fed dual three-phase induction machine with open-end windings configuration under post-fault condition was investigated in this paper. The quad-inverter scheme is capable to generate multi-level voltage waveforms

during healthy state, equivalent to the ones of a three-level inverter, and it is able to share the total motor power among the four dc sources within each switching period with three degree of freedom. It has been shown that during post-fault operating conditions, with one failed inverter, the power rating is reduced to the half, and one degree of freedom in the power sharing is lost. More specifically, the remaining two degrees of freedom can be exploited to equally share the total motor power between the two three-phase motor windings, leading to optimum motor and inverter efficiency, or among the three remaining dc sources, leading to a balanced charge status of the used batteries.

Numerical implementation and results provided in this paper show good agreement with theoretical analysis. The hardware prototype of the whole ac motor drive system is actually under development at the Power Electronics Lab of Dept. of Electrical Engineering, University of Bologna (IT).

References

[1] A.H. Bonnett, C. Yung, Increased efficiency versus increased reliability, IEEE. Ind. App. Mag. 14 (1) (2008) 29-36.

[2] A. Siddique, G.S. Yadava, B. Singh, A review of stator fault monitoring techniques of induction motors, IEEE Tran. on Ener. Conv. 20 (1) (2005) 106-114.

[3] A. Bellini, F. Filippetti, C. Tassoni, G.A. Capolino, Advances in diagnostic techniques for induction machines, IEEE Trans. on Ind. Electron. 55 (12) (2008) 4109-4126.

[4] E. Levi, Multiphase electric machines for variable-speed applications, IEEE Trans. on Ind. Appl. 55 (5) (2008) 1893-1909.

[5] G. Grandi, G. Serra, A. Tani, General analysis of multiphase systems based on space vector approach, in: Proc. Inter. Power Electron. and Motion Control Conf., EPE–PEMC' 06, Portoroz, Slovenia, Aug. 30-Sept. 1, 2006, pp. 834-840.

[6] J. Rodriguez, S. Bernet, B. Wu, J.O. Pontt, S. Kouro, Multilevel voltage-source-converter topologies for industrial medium-voltage drives, IEEE Trans. on Ind. Electron 54 (6) (2007) 2930-2945.

[7] L.G. Franquelo, J. Rodriguez, J.I. Leon, S. Kouro, R. Portillo, M.M. Prats, The age of multilevel converters arrives, IEEE Ind. Electron. Magazine 2 (2) (2008) 28-39.

[8] S. Bolognani, M. Zordan, M. Zigliotto, Experimental fault-tolerant control of a PMSM drive, IEEE Trans. on Ind. Electron. 47 (5) (2000) 1134-1141.

[9] R.L. de A. Ribeiro, C.B. Jacobina, E.R.C. da Silva, A.M.N. Lima, Fault-tolerant voltage-fed PWM inverter ac motor drive systems, IEEE Trans. on Ind. Electron. 51 (2) (2004) 439-446.

[10] A.L. Julian, G. Oriti, A comparison of redundant inverter topologies to improve voltage source inverter reliability, IEEE Trans. on Ind. Appl. 43 (5) (2007) 1371-1378.

[11] S. Yang, A. Bryant, P. Mawby, D. Xiang, Li Ran, P. Tavner, An industry-based survey of reliability in power electronic converters, IEEE Trans. on Ind. Electron. 47 (3) (2011) 1441-1451.

[12] S. Yang, D. Xiang, A. Bryant, P. Mawby, Li Ran, P. Tavner, Condition monitoring for device reliability in power electronic converters: A review, IEEE Trans. on Power Electron. 25 (11) (2010) 2734-2752.

[13] Y. Zhao, T.A. Lipo, Space vector PWM control of dual three-phase induction machine using vector space decomposition, IEEE Trans. on Ind. Appl. 31 (5) (1995) 1100-1109.

[14] G. Grandi, A. Tani, G. Serra, Space vector modulation of six-phase VSI based on three-phase decomposition, in: Conf. Proc. IEEE 19th Symposium on Power Electron., Electrical Drives etc., SPEEDAM' 08, Taormina, Italy, June 11-13, 2008, pp. 674-679.

[15] Y. Kawabata, M. Nasu, T. Nomoto, E.C. Ejiogu, T. Kawabata, High-efficiency and low acoustic noise drive system using open-winding AC motor and two space-vector-modulated inverters, IEEE Trans. on Ind. Electron. 49 (4) (2002) 783-789.

[16] J. Kim, J. Jung, K. Nam, Dual-inverter control strategy for high-speed operation of EV induction motors, IEEE Trans. on Ind. Electron. 51 (2) (2004) 312-320.

[17] R. Kanchan, P. Tekwani, K. Gopakumar, Three-level inverter scheme with common mode voltage elimination and dc link capacitor voltage balancing for an open-end winding induction motor drive, IEEE Trans. on Power Electron. 21 (6) (2006) 1676-1683.

[18] G. Grandi, C. Rossi, A. Lega, D. Casadei, Multilevel operation and input power balancing for a dual two-level inverter with insulated dc sources, IEEE Trans. on Ind. Appl. 44 (6) (2008) 1815-1824.

[19] R. Bojoi, A. Tenconi, F. Farina, F. Profumo, Dual-source fed multi-phase induction motor drive for fuel cell vehicles: topology and control, in: Proc. of 36th Power Electron., Specialists Conf., PESC' 05, Recife, Brazil, June 16-16, 2005, pp. 2676-2683.

[20] D.G. Holmes, T.A. Lipo, Pulse Width Modulation for Power Converters: Principles and Practice, IEEE Press-John Wiley, 2003, pp. 467-469.

[21] G. Grandi, A. Tani, P. Sanjeevikumar, D. Ostojic, Multi-phase multi-level AC motor drive based on four three-phase two-level inverters, in: Conf. Proc. IEEE 20th Symposium on Power Electron., Electrical Drives etc., Pisa, Italy, June 14-16, 2010, pp. 1768-1775.

[22] G. Grandi, Y. Gritli, F. Filippetti, C. Rossi, Fault-tolerant operating analysis of a quad-inverter multiphase multilevel ac motor drive, in: Conf. Proc. SDEMPED'11, Bologna, Italy, Sept. 5-8, 2011, pp. 126-132.

[23] G. Grandi, P. Sanjeevikumar, Y. Gritli, F. Filippetti, Experimental investigation of fault-tolerant control strategies for quad-inverter converters, in: Conf. on Electrical Systems for Aircraft, Railway and Ship Propulsion, ESARS 2012, Bologna, Italy, Oct. 16-18, 2012, pp. 1-8.